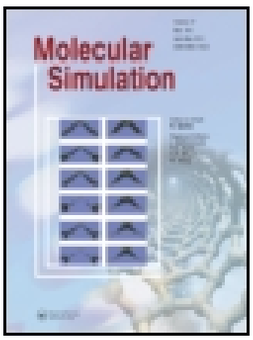

Molecular Simulation

ISSN: 0892-7022 (Print) 1029-0435 (Online) Journal homepage: http://www.tandfonline.com/loi/gmos20

Removal of arsenic ions using hexagonal boron nitride and graphene nanosheets: a molecular dynamics study

R. Srivastava, A. Kommu, N. Sinha & J. K. Singh

To cite this article: R. Srivastava, A. Kommu, N. Sinha & J. K. Singh (2017): Removal of arsenic ions using hexagonal boron nitride and graphene nanosheets: a molecular dynamics study, Molecular Simulation, DOI: 10.1080/08927022.2017.1321754

To link to this article: http://dx.doi.org/10.1080/08927022.2017.1321754

Published online: 30 May 2017.

MOLECULAR SIMULATION, 2017
https://doi.org/10.1080/08927022.2017.1321754

Taylor & Francis
Taylor & Francis Group

Removal of arsenic ions using hexagonal boron nitride and graphene nanosheets: a molecular dynamics study

R. Srivastava[a], A. Kommu[a], N. Sinha[b] and J. K. Singh[a]

[a]Department of Chemical Engineering, Indian Institute of Technology Kanpur, Kanpur, India; [b]Department of Mechnical Engineering, Indian Institute of Technology Kanpur, Kanpur, India

ABSTRACT

The presence of high concentration of arsenic in conventional water sources can cause serious health and environmental hazards. An urgent need is to find an efficient adsorbent for the removal of arsenic ions (As^{3+}) from contaminated water. In the present study, molecular dynamics simulation is used to understand the adsorption behaviour of As^{3+} on hexagonal boron nitride (*h*-BN) and graphene nanosheets. The adsorption of As^{3+} follows the Langmuir isotherm and the maximum adsorption capacities are found to be 270.1 and 211.7 mg/g for *h*-BN and graphene nanosheets, respectively. Further, potential of mean force (PMF) of As^{3+} revealed that the *h*-BN nanosheet possesses lower contact minima (−1.35 kcal/mol) for arsenic ion compared to graphene nanosheet (−1.2 kcal/mol). These results indicate strong interaction between arsenic ion and *h*-BN nanosheet. On the other hand, desorption of As^{3+} on *h*-BN nanosheet showed higher energy barriers (2.3 kcal/mol) compared to graphene nanosheet (1.5 kcal/mol). Correspondingly, the residence time of As^{3+} is approximately threefold higher on *h*-BN nanosheet compared to graphene nanosheet. We also report that the presence of partial charges on B and N atoms in the *h*-BN sheet influence the adsorption behaviour As^{3+} ions and the maximum adsorption capacity of *h*-BN nanosheet with partial charges is found to be 311.7 mg/g. Thus, our study strongly suggests the potential applicability of *h*-BN nanosheet as an efficient adsorbent for the removal of arsenic ions.

ARTICLE HISTORY
Received 23 November 2016
Accepted 14 April 2017

KEYWORDS
Boron nitride; graphene; arsenic; adsorption; molecular dynamics

1. Introduction

In the past decades, the population growth in the world has boomed. As a consequence, there is an increasing demand for fresh water supply. The conventional sources such as rivers, lakes, ground water, etc. are being exploited to fulfil this demand, and are further worsened by industrial development which are contributing to water pollution. The presence of heavy metals ions, such as Pb^{2+}, Cu^{2+}, As^{3+}, Cr^{4+}, Hg^{2+} and Zn^{2+}, in industrial wastewater has been a great concern on the environment and human health. Thus, there is a need for treatment of industrial and municipal wastewater to protect our conventional water sources from pollutants. Arsenic is one of the common water pollutant having serious health concerns.

In natural fresh water sources, concentration of arsenic is less than 1–2 μg/L and the World Health Organization (WHO) has recommended up to 10 μg/L arsenic in drinking water [1]. Several countries, including India, Bangladesh, China, USA, Australia, Pakistan, Vietnam, Nepal and South America are facing problem of arsenic concentration above 10 μg/L in groundwater and more than 100 million population are affected with it [2–5]. Long time usage of arsenic contaminated water may lead to severe health problems such as arsenicosis, dermal lesions, peripheral neuropathy, and bladder, lung and skin cancers [1,6,7].

Several techniques are used for the removal of arsenic from water. This includes membrane filtration, coagulation-precipitation, ion-exchange, adsorption and bio-remediation [7–11]. Among all these techniques, adsorption method is considered to be most efficient for the removal of metal ions from water [8,9,12]. Several adsorbents such as activated carbons, clay minerals, polymer resin, biosorbents and metal oxides, etc. are used for the removal of arsenic from water [7,11,13]. The arsenic (As^{3+}) adsorption capacity of some suitable absorbents are presented in Figure 1 [14–18]. Various chemical modifications have been attempted to enhance the adsorption capacity. For example, chemically modified saw-dust with La and Zr oxide has been used for the removal of As^{3+} and As^{5+} ions from water [16]. Iron-modified activated carbon has been applied as an absorbent for the removal of arsenic ions from aqueous solution, achieving the adsorption capacity of 43–51 mg/g for As^{3+} and 38–39 mg/g for As^{5+} at different pH [19]. The increase in saturation capacity of monolayer As^{3+} with increasing temperature has been reported on Fe–Mg hydrotalcite [20]. Iron-oxide nanoparticle coated with titanium oxide (Fe_3O_4@TiO_2 nanoparticle) has been used to remove arsenic ions from water in environmental conditions [21]. A novel hybrid material zirconium polyacrylamide (ZrPACM-43) for the adsorption of As^{3+} ions has been reported by Mandal et al. [22] with the Langmuir adsorption capacity of 41.48 mg/g for As^{3+}. However, these adsorbents suffer from some drawbacks of low adsorption capacities, poor selectivity and costly regeneration [7,23–25]. Therefore, it is highly desirable to find low-cost alternative adsorbents that exhibit high adsorption capacities, selectivity and rapid regeneration.

CONTACT J. K. Singh jayantks@iitk.ac.in

Among most of the inorganic nanomaterials, carbon-based materials have attracted attention from several researchers owing to its unique properties such as high porosity, large specific surface area, high chemical, thermal and mechanical stability. Therefore the carbon-based materials are used as nanomembranes for removal of organic pollutants from wastewater. The chemically modified carbon nanotubes with functional groups acts as adsorption sites for pollutants [26–28]. In spite of these advantages, it is challenging to synthesise highly aligned carbon nanotubes which limits their commercial usage [29]. Graphene has been considered as superior adsorbent for the removal of various environmental pollutants from wastewater, is economical and has novel properties similar to carbon nanotubes. Zhao et al. [30], developed the graphene sponge and performed adsorption and desorption study for various water contaminations such as dyes, oils and many other organic solvents. Wu et al. [31], studied removal of hazardous chemicals in wastewater using graphene. While these studies show enhanced adsorption for organic pollutants such as acrylonitrile and methyl blue on graphene, the work of Mishra and Ramaprabhu [32] shows that graphene sheets can be used to remove of high concentration of inorganic species like arsenic and sodium ions from aqueous solution.

The popularity gained by the graphene sheet as an adsorbent for metal ions and organic pollutants from aqueous solution has also insinuated the suitability of hexagonal boron nitride, a structural analogue of graphene, for similar applications. A hexagonal boron nitride is composed of alternating B and N atoms substituting C atoms in a graphene sheet with almost similar atomic spacing. In recent years, hexagonal boron nitride (*h*-BN) nanosheet, have gained considerable attention due to their exceptional properties such as resistance to oxidation, large surface area, wide band gap, high mechanical, thermal and chemical stability [33–35]. These properties make *h*-BN nanosheet suitable material for various technological applications, including electronic devices [36], ultraviolet light emitting devices [37], catalyst support [38,39] and lithium batteries [40].

Several studies have shown the potential of boron nitride (BN) in adsorbing contaminants from aqueous solutions. Fluorinated activated boron nitride (F-ABN) [41] has been used for effective and rapid removal of Cr^{3+} ion from aqueous solution with high adsorption capacity (387 mg/g). Li et al. [42,43] reported that activated boron nitride is effective for the removal of metal ions and organic pollutants from wastewater. They found the maximum adsorption capacities of Co^{2+}, Ni^{2+}, Ce^{3+} and Pb^{2+} as 215, 235, 282 and 225 mg/g, respectively, on activated BN and concluded that the adsorption capacities of activated BN is significantly higher than activated carbon. Zhang et al. [44] observed high adsorption rate and capacity of BN nanocarpets for methylene blue. The porous BN nanosheet is found to be effective in adsorbing oils, organic solvents and dye from water [45]. Chen et al. [46] have functionalised BN nanotube with Fe_3O_4 nanoparticles and used it for the adsorption of arsenic ions (As^{5+}) from water solutions. They reported that the functionalised multi-walled boron nitride nanotube (BNNT) possessing high surface area is suitable for the adsorption of As^{5+} ions and the maximum As^{5+} ion adsorption capacity of functionalised BNNT was estimated to be 32.2 mg/g. Recent study by Garnier et al. [29] shows permeation of water through nanoporous graphene and BN membranes. They reported higher water permeability through the BN monolayer membrane, which is mainly due to decrease in surface tension of water near BN membrane in comparison to graphene membrane. However, to the best of our knowledge, the application of *h*-BN nanosheet for the removal of As^{3+} is lacking. Efforts are needed to understand adsorption mechanism of As^{3+} on *h*-BN nanosheet.

In natural conditions, arsenic mainly exits in two forms, arsenite (As^{3+}) and arsenate (As^{5+}) in water [47]. It is well known that toxicity of (As^{3+}) is several order higher than that of (As^{5+}). Further, its lower affinity towards various adsorbents make it difficult to extract from aqueous solutions [47–49]. The aim of this work is to provide insight into the adsorption behaviour of As^{3+} on *h*-BN and graphene nanosheets using molecular dynamics simulations. Also the current work explores the structural and dynamic behaviour of As^{3+} ions near the *h*-BN and graphene nanosheets.

2. Simulation details

2.1. Potential model

In the present study, hexagonal boron nitride (*h*-BN) and graphene nanosheets are constructed using nanostructure builder plug-in in Visual Molecular Dynamics package [50]. The single layer rectangular sheet of hexagonal boron nitride (*h*-BN) and graphene nanosheets are considered with approximate dimensions 52.0 and 43.0 Åin x and y directions, respectively. The system considered as an aqueous solution of $As(NO_3)_3$ ionic salt on the top (in z direction) of the nanosheets at various concentrations. The boron and nitrogen atoms in *h*-BN [51] and carbon in graphene [52] nanosheets are modelled as uncharged and kept rigid. TIP3P model is used to describe water interactions [53], the force field parameters for As^{3+} ions are taken from universal force field [54], and flexible model of NO_3^- ions is considered [55,56]. The force field parameters used in the present study are tabulated in Table 1. The non-bonded interactions are defined by Lennard-Jones (LJ) and Coulombic potentials

$$U_{\text{nonbonded}}(r_{ij}) = 4\epsilon_{ij}\left[\left(\frac{\sigma_{ij}}{r_{ij}}\right)^{12} - \left(\frac{\sigma_{ij}}{r_{ij}}\right)^{6}\right] + \frac{q_i q_j}{4\pi\epsilon_0 r_{ij}}, \quad (1)$$

where σ_{ij} and ϵ_{ij} are the size and energy parameters; q_k and ϵ_0 are the partial charge on k^{th} atom and permittivity of free space, respectively; r_{ij} is the distance between the pair of atoms. The nanosheet-water and nanosheet-ion interactions are described by LJ potential and the corresponding interaction parameters between dissimilar interaction sites are calculated using the Lorentz–Berthelot mixing rules.

Bond stretching for the – NO_3^- ions is described by a harmonic potential [57]

$$U_{\text{stretching}} = \frac{1}{2}k_l(l - l_0)^2, \quad (2)$$

where l is the bond length, l_0 is the equilibrium bond length and k_l is the bond force constant and the bond bending is expressed by

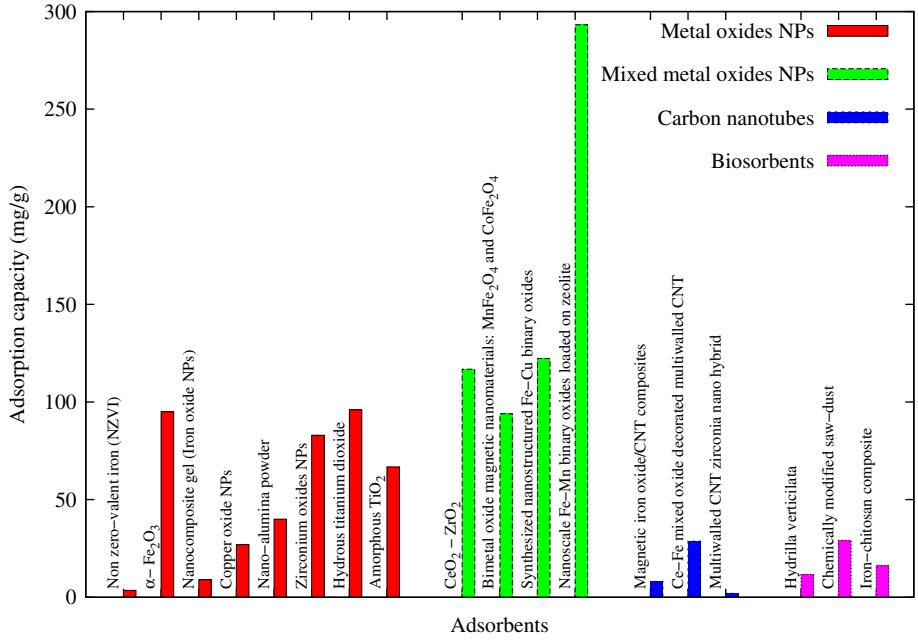

Figure 1. (Colour online) Adsorption capacity of various adsorbents for the removal of arsenic ions (As^{3+}) [14–18].

Table 1. Force field parameters.

Molecules/ions	Site	Charge	σ (Å)	ϵ (kcal/mol)
water	O	−0.834	3.1506	0.1521
	H	0.417	0.0000	0.0000
$-NO_3^-$	N	0.950	3.2070	0.1600
	O	−0.650	3.3490	0.1700
arsenic ion	As^{3+}	3.000	4.2300	0.3090
h-BN	B	0.000	3.4530	0.0950
	N	0.000	3.3650	0.1448
graphene	C	0.000	3.4000	0.0556

$$U_{\text{bending}} = \frac{1}{2}k_\theta(\theta - \theta_0)^2, \tag{3}$$

where k_θ is the angle force constants, θ is the angle and θ_0 is the equilibration angle.

2.2. Simulation method

All the molecular dynamics simulations are carried out using the LAMMPS [58] package. Initially the simulation system is generated by performing NPT simulation on a mixture of arsenic nitrate salt ($As(NO_3)_3$) and water for 1ns at a constant 1 atm pressure, and 298 K temperature. Then the equilibrated ionic solution is placed 8 Å above the nanosheets (see Figure 2). The periodic boundary conditions are applied in three spatial directions, with 100 Å vacuum above the aqueous solution along the $z-$direction. The simulation system considered in this study consists of 3000 water molecules with varying the number of As^{3+} ions from 3 to 38 depending on ion concentration, and are placed randomly in the aqueous solution. The simulations are carried out in the canonical (NVT) ensemble with the Nosé Hoover thermostat to maintain temperature at 298 K. Particle particle particle mesh technique is applied to compute long-range interactions. The system is equilibrated for 5 ns with an integration time step of 1 fs, followed by the production run of 5 ns.

Trajectories of the system obtained from molecular dynamic (MD) simulations are used to calculate the structural, dynamical and the adsorption capacity of As^{3+} ions on *h*-BN and graphene nanosheets. The density profiles (ρ) of water and As^{3+} ions are calculated in z direction above the nanosheet for different concentrations of As^{3+} ions in aqueous solution. The time correlation function $C(t)$ of monolayer of water/As^{3+} ions near the nanosheet is defined as [56]

$$C(t) = \frac{\langle\theta(t)\theta(0)\rangle}{\langle\theta(0)\theta(0)\rangle} = A\exp(-t/\tau), \tag{4}$$

where $\theta(t) = 1$, if water/As^{3+} ion is present in the monolayer near the nanosheet, and τ is the residence time.

The diffusion coefficients (D) of water and As^{3+} ions within the monolayer near the nanosheet between time 0 and t are calculated by considering the mean-square displacement (MSD) [59,60]

$$\text{MSD} = \frac{\langle[\Delta x^2(t) + \Delta y^2(t)]S^{\text{mono}}(t)\rangle}{4t\langle S^{\text{mono}}(t)\rangle}, \tag{5}$$

$$D_{II}(z_{\text{mono}}) = \frac{1}{4}\lim_{t\to\infty}\frac{\text{d}}{\text{d}t}(\text{MSD}), \tag{6}$$

where $\Delta x^2 = [x(t) - x(0)]^2$ along x (similarly for y), z_{mono} represents the monolayer near the nanosheet and $S^{\text{mono}}(t) = 1$ if the water/As^{3+} ions remains continuously in the monolayer near the nanosheet between 0 to t, while $S^{\text{mono}}(t) = 0$ otherwise. The error is estimated by taking standard deviation on block average of the diffusion coefficient over the sampling time [61]. The amount adsorbed by the ions on the substrate is quantified by the Langmuir isotherm which is given by [62]

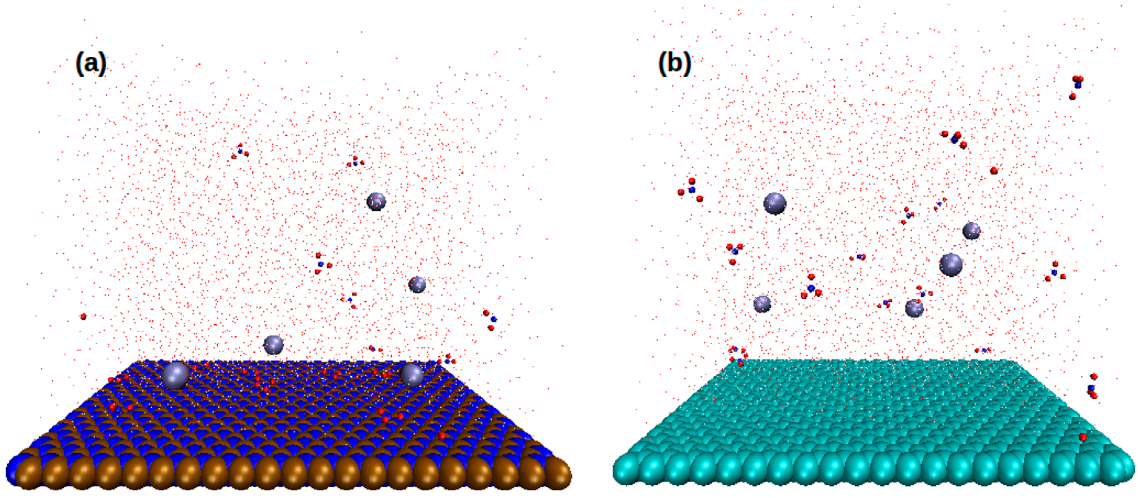

Figure 2. (Colour online) Snapshot of the system containing aqueous solution of 0.1 M arsenic nitrate salt ($As(NO_3)_3$) above the *h*-BN nanosheet (panel a) and graphene nanosheet (panel b).

$$q_a = q_m\left(\frac{Kc_e}{1+Kc_e}\right), \tag{7}$$

where q_a and q_m are the amount adsorbed and the maximum amount of adsorption of ions on the nanosheet, respectively. The equilibrium ion concentration and the Langmuir equilibrium constants are denoted by c_e and K, respectively.

One of the essential features of Langmuir isotherm can be described by equilibrium parameter R_L, which is a dimensionless constant and is defined as [63,64]

$$R_L = \frac{1}{1+Kc}, \tag{8}$$

where c is the initial concentration of adsorbate. The value of R_L shows the nature of the adsorption isotherm, $0 < R_L < 1$ indicates favourable, $R_L > 1$ unfavourable, $R_L = 1$ linear and $R_L = 0$ irreversible adsorption.

The effective interaction strength between the ion and the nanosheet has been quantified by the potential mean force (PMF) which is calculated using umbrella sampling method [65,66]. The umbrella sampling method imposes a harmonic potential to constrain the motion of arsenic ion along the z-direction perpendicular to the nanosheet, while the arsenic ion was free to move in the other two directions. In this work, the mean force distribution is obtained by sampling the harmonic force experienced by the arsenic ions which are placed at different positions along the z-axis, from bulk solution phase to the adsorbed phase. The PMF is generated by the umbrella sampling using large number of windows that covers the whole range of distances from solution phase to the adsorbed phase with a sufficient overlap between adjacent windows. The harmonic biasing potential $K_z(z-z_i)^2/2$, where z is the distance between the arsenic ion and the nanosheet, z_i denotes the target position from the nanosheet and K_z is the force constant. In order to construct the PMF between the nanosheet and arsenic ion as a function of separation distance z, biased simulations are performed with target position varied from $z = 20$ to 1 Å, with a decrement of 1 Å. The harmonic biasing force constant $K_z = 2$ kcal/mol Å^2 is applied for all windows, with sufficient overlapping of histograms. The biased data from umbrella histogram are analysed using the weighted histogram analysis method [65] (WHAM) to estimate PMF.

3. Results and discussions

We started the investigation by calculating density profile of water, and arsenic ions along z direction above the *h*-BN and graphene nanosheets. The density profiles of water are plotted in Figure 3(a) and (b) for different ion concentrations c (mol/L) on *h*-BN, and graphene nanosheets, respectively. It is observed that water molecules form layers near both the nanosheets. It is also clear from Figure 3 that density of first layer is greater than that of layers above it, which is primarily due to the surface–fluid interactions and packing effect [67]. This is akin to the behaviour seen by earlier workers on wetting behaviour of water on boron nitride and graphite nanosheets [68,69]. Zoomed inset of Figure 3 suggests that the water density of first layer decreases with increase in ion concentration, c, on both the nanosheets. This is due to the accumulation of arsenic ions near the nanosheets which can be observed from arsenic ion density profile near the nanosheet discussed later in this section. We clearly observed that the first layer water density above the *h*-BN nanosheet is greater than that on the graphene nanosheet, indicating strong interaction between water and *h*-BN compared to the water and graphene. Similar to water, the density profile of arsenic ions showed layering near the *h*-BN and graphene nanosheets (Figure 4(a) and (b)). It has been shown in Figure 4(a) that the density of first layer of As^{3+} ions increases with increasing ion concentration, which represents enhanced adsorption of arsenic ions with increasing ion concentration on *h*-BN nanosheet. Similar observation of increasing first layer density of arsenic ion with increasing ion concentration has been observed on the graphene nanosheet. It has been clearly shown in Figure 4(a) and (b) that the first layer density of arsenic ions on *h*-BN nanosheet is several times greater than that on graphene nanosheet.

It is well known that the adsorption isotherm can provide information related to intensity of the interaction between

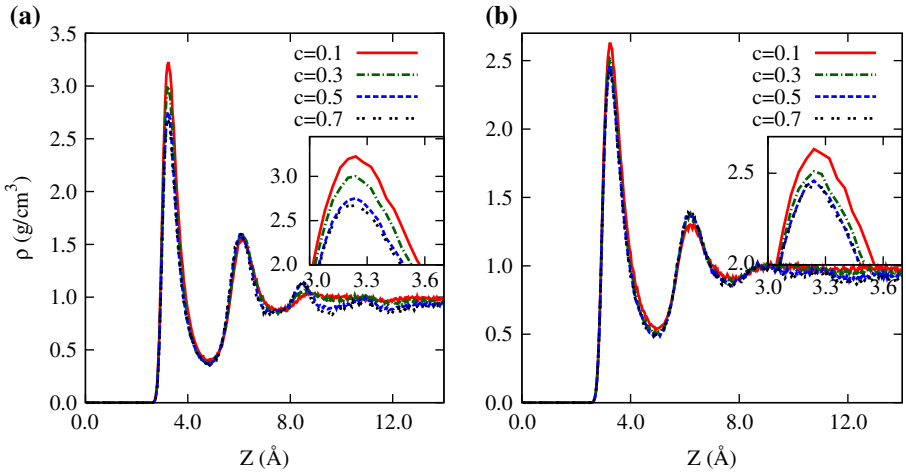

Figure 3. (Colour online) Density profile of water in *z* direction above the *h*-BN nanosheet (panel a) and graphene nanosheet (panel b) at different ion concentrations *c* (mol/L).

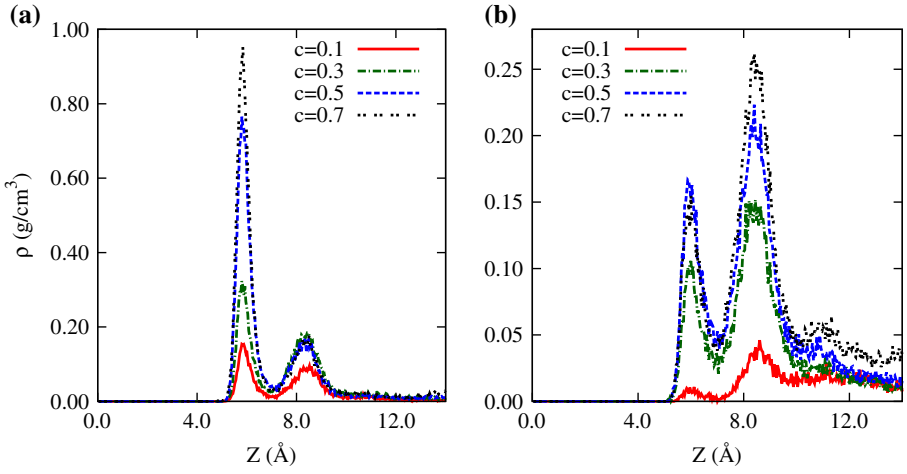

Figure 4. (Colour online) Density profile of arsenic ions in *z* direction above the *h*-BN nanosheet (panel a) and graphene nanosheet (panel b) at different ion concentrations *c* (mol/L).

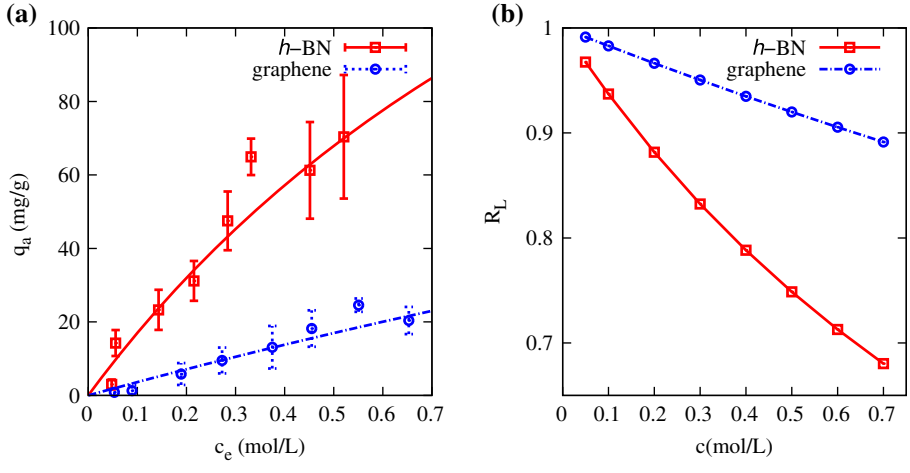

Figure 5. (Colour online) The Langmuir adsorption isotherm of arsenic ions (As^{3+}) (panel a) and equilibrium parameter (R_L) as a function of ion concentration (*c*) (panel b).

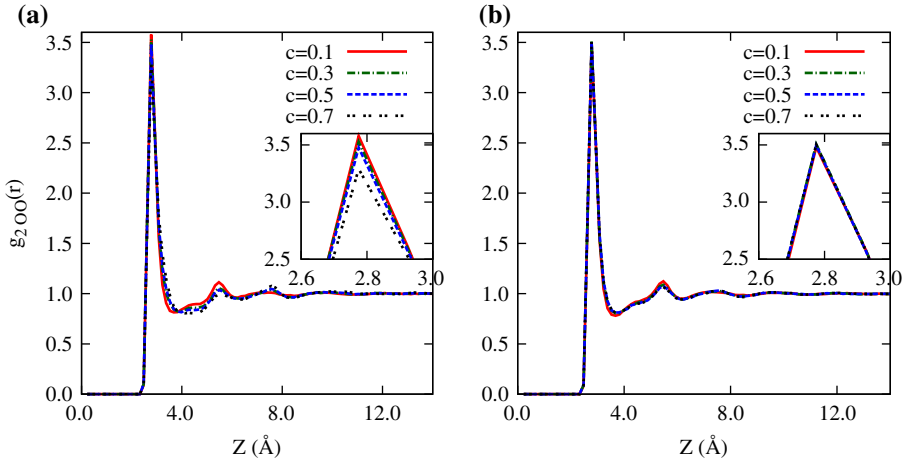

Figure 6. (Colour online) The two-dimensional radial distribution function of the monolayer of water ($g_{2OO}(r)$) at different ion concentrations c (mol/L) on h-BN nanosheet (panel a) and graphene nanosheet (panel b).

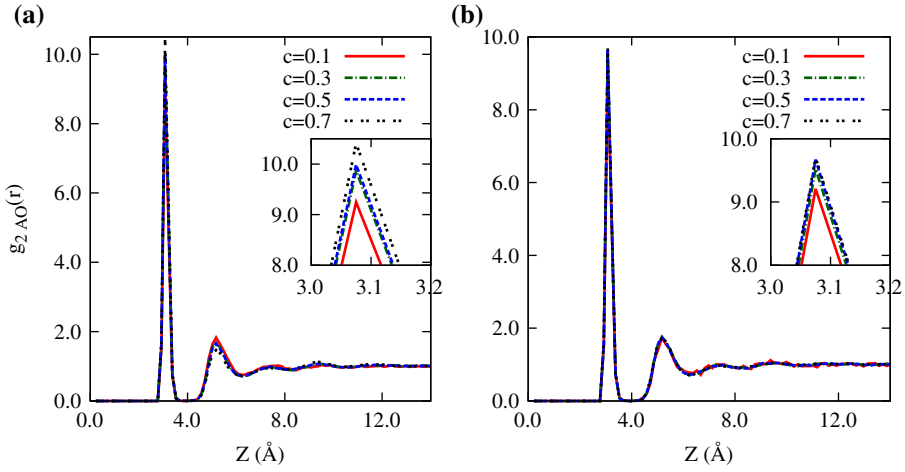

Figure 7. (Colour online) The two-dimensional radial distribution function of the monolayer of arsenic-water ($g_{2AO}(r)$) at different ion concentrations c (mol/L) on h-BN nanosheet (panel a) and graphene nanosheet (panel b).

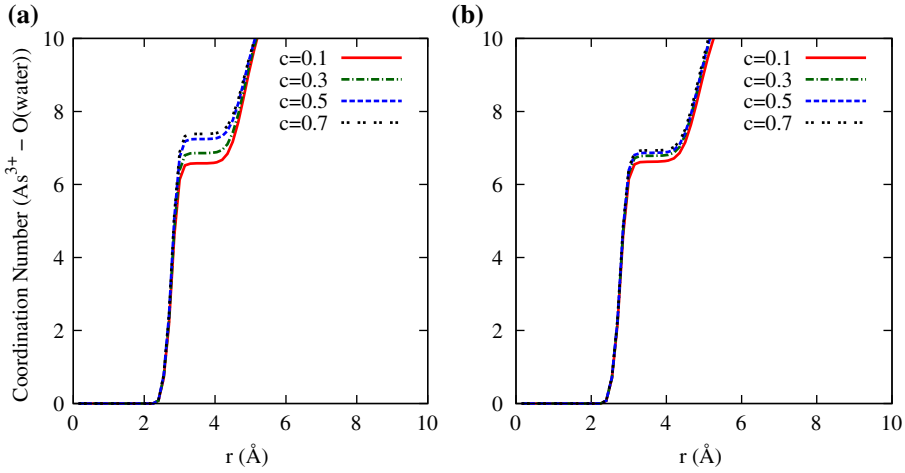

Figure 8. (Colour online) The hydration of arsenic ions at different ion concentrations c (mol/L) in the monolayer near h-BN nanosheet (panel a) and graphene nanosheet (panel b).

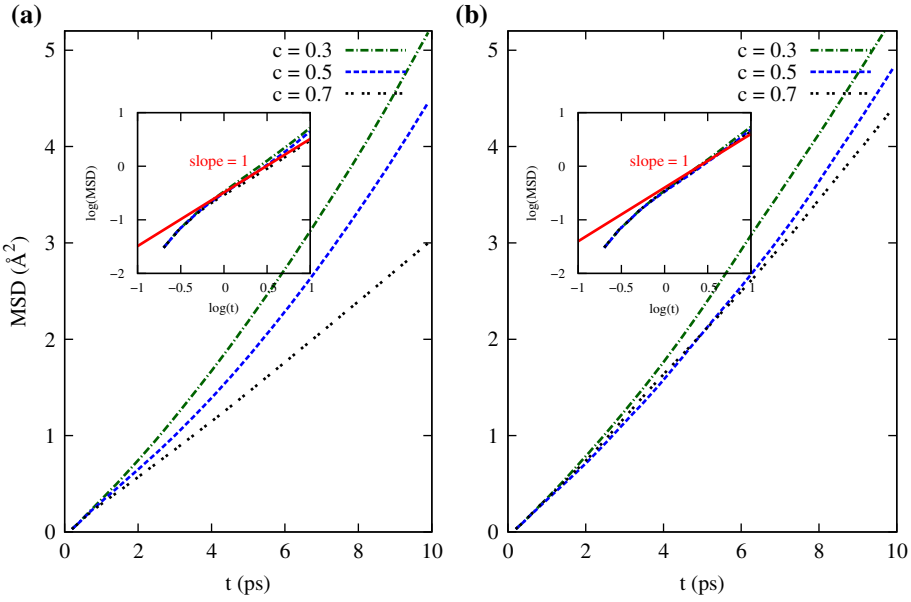

Figure 9. (Colour online) The two-dimensional mean square displacement of arsenic ion within the monolayer near the *h*-BN (panel a) and graphene nanosheet (panel b). log–log plot of the MSD is shown in the inset using the same line styles for the different ion concentrations. Straight line of slope = 1 has been included as an aid in identifying the diffusive regime.

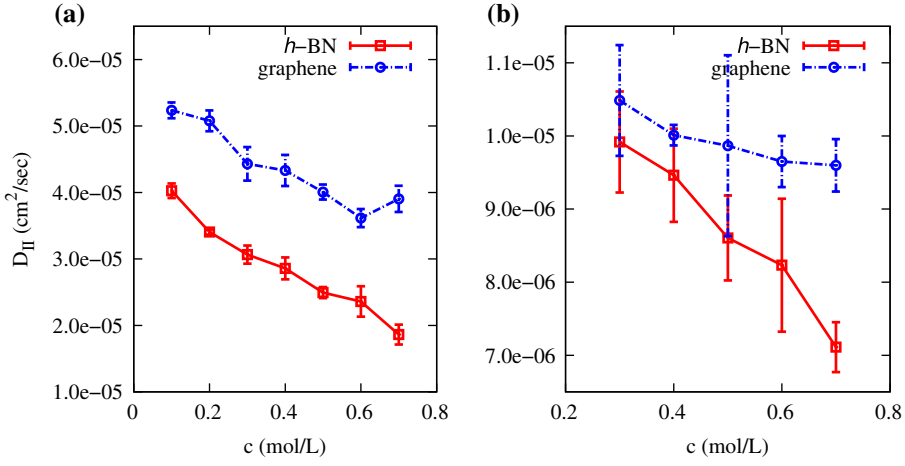

Figure 10. (Colour online) The two-dimensional diffusion coefficient of water (panel a) and arsenic ions (panel b) on *h*-BN nanosheet and graphene nanosheets as a function ion concentration *c* (mol/L).

adsorbate and adsorbent. Therefore, in order to understand adsorption behaviour of arsenic ions on *h*-BN and graphene nanosheets, we have fitted the Langmuir adsorption isotherm equation to compute various adsorption parameters. The Langmuir model assumes that the monolayer adsorption occurs on a homogeneous surface. Thus, we consider the ions present in the first monolayer near the nanosheet as adsorbed ions and plotted the mass adsorbed ions per unit mass of nanosheet, q_a (mg/g) as a function of equilibrium ion concentration, c_e (mol/L)) in Figure 5(a) at a temperature 298 K. Figure 5(a) shows the increase in mass of adsorbed arsenic ions with increasing equilibrium ion concentration c_e for both the nanosheets. It is also seen from Figure 5(a) that the adsorption of arsenic ion is more on *h*-BN nanosheet compared to the graphene nanosheet, which is also reflected from the density profile of As^{3+} ion where the height of first peak is several times higher for the *h*-BN nanosheet (see Figure 4). It is also observed from Figure 5(a) that the adsorption isotherms for both the cases fits well with the Langmuir isotherm. The maximum arsenic ion adsorption capacities (q_m), estimated by the Langmuir isotherm equation on *h*-BN and graphene nanosheets are 270.1 and 211.7 mg/g, respectively. A comparison with the adsorption data available in the literature as shown in Figure 1 clearly suggests that the maximum adsorption capacity of As^{3+} ion on *h*-BN nanosheet obtained in this study are competitive with various adsorbents. Equilibrium parameter R_L are calculated from Equation (8) for both the nanosheets at different ion concentrations and plotted in Figure 5(b). The decrease in R_L values with increasing ion concentration (c) indicates favourable adsorption at higher ion concentration. It is also evident from Fig 5(b) that the

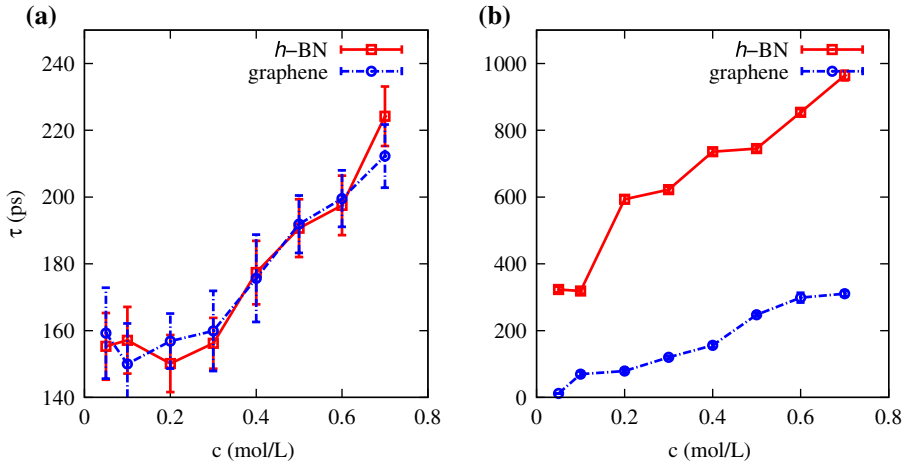

Figure 11. (Colour online) The residence time (τ) of water (panel a) and arsenic ions (panel b) on *h*-BN and graphene nanosheets at different ion concentrations *c* (mol/L).

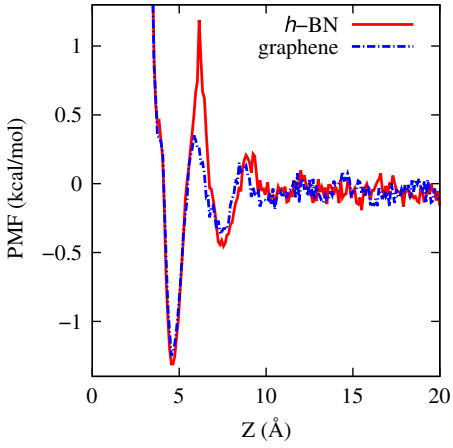

Figure 12. (Colour online) The potential mean force on arsenic ions by *h*-BN and graphene nanosheets as a function of perpendicular distance from the nanosheet *z*.

arsenic ion adsorption is more favourable on *h*-BN nanosheet in comparison to graphene nanosheet.

In order to investigate influence of nanosheets on structural properties of water and ions, we computed two-dimensional radial distribution function($g_2(r)$). Figure 6(a) and (b) shows the in-plane radial distribution function (rdf) of water–water ($g_{2_{OO}}(r)$) on *h*-BN and graphene nanosheets, respectively. The in-plane radial distribution is calculated using monolayer of water above the *h*-BN or graphene nanosheet. Figure 6(a) shows that the height of first peak of the in-plane rdf decreases with increasing ion concentration *c* for *h*-BN nanosheet. This indicates water density in the monolayer which decreases with increase in *c*, which is also seen from Figure 3(a). This is primarily due to increase in occupation of As^{3+} ions in the monolayer as clearly seen in Figure 4(a), whereas the effect of ion concentration on $g_{2_{OO}}(r)$ for graphene nanosheet is negligible. The two-dimensional rdf of arsenic–water ($g_{2AO}(r)$) is computed within the monolayer near both the nanosheets, and are plotted in Figure 7(a), and (b) for *h*-BN, and graphene nanosheets, respectively. We observed the height of first peak of $g_{2AO}(r)$ increases with increasing ion concentration in aqueous solution in both the nanosheets. It is also seen that the first peak and second peak are around 3.07, and 5.2 Å, respectively. The first peak height ($g_{2AO}(r)$) is more pronounced in case of *h*-BN nanosheet compared to graphene nanosheet. To quantify the increment in the first peak height of $g_{2AO}(r)$ with ion concentration within the monolayer near both the nanosheets, we computed coordination number of arsenic ions in solvation shell by integrating the in-plane radial distribution function $g_{2AO}(r)$. Figure 8 shows the coordination number of arsenic ions in the solvation shell increases with increasing ion concentration near both the nanosheets and the number of arsenic ions are more near the *h*-BN nanosheet with increasing ion concentrations.

To understand the effect of *h*-BN and graphene nanosheets on dynamical behaviour of water and ions in aqueous solution, we computed the mean square displacement (MSD) within the monolayer near the nanosheet. Figure 9 shows the MSD of arsenic ions near the nanosheets at various ion concentrations. It is observed from Figure 9(a) that the MSD of arsenic ions near *h*-BN decreases with increase in ion concentrations. Similar to *h*-BN nanosheet, the MSD of arsenic ions also decreases near graphene nanosheet with increase in ion concentration. It is also evident from Figure 9 that the MSD of arsenic ion is lower near *h*-BN compared to graphene nanosheets. In inset of Figure 9, we have shown the log–log plot of the MSD which represents the diffusive regime of molecules where the slope is equal to 1. In the present study, we calculated the diffusion coefficient of water and ions within the monolayer near the nanosheet. The value of monolayer diffusion coefficient indicates the strength of interaction between the molecule and nanosheet while it is adsorbed. Figure 10(a) shows the diffusion coefficient (D_{II}) of water molecules within the monolayer near the *h*-BN and graphene nanosheets. It has been observed that there is a decreases in monolayer diffusion with increase in ion concentration on both nanosheets. It is also evident from Figure 10(a), that the monolayer diffusion of water is less on *h*-BN nanosheet compared to that on the graphene nanosheet. Similar to water the monolayer diffusion coefficient of As^{3+} ions also decreases with increase in ion concentration on both the nanosheets (Figure 10(b)). The decrease in monolayer diffusion coefficient with increasing ion concentration is more on *h*-BN nanosheet, which indicates higher adsorption of As^{3+} ions on *h*-BN nanosheet with increasing *c*. This is also verified from

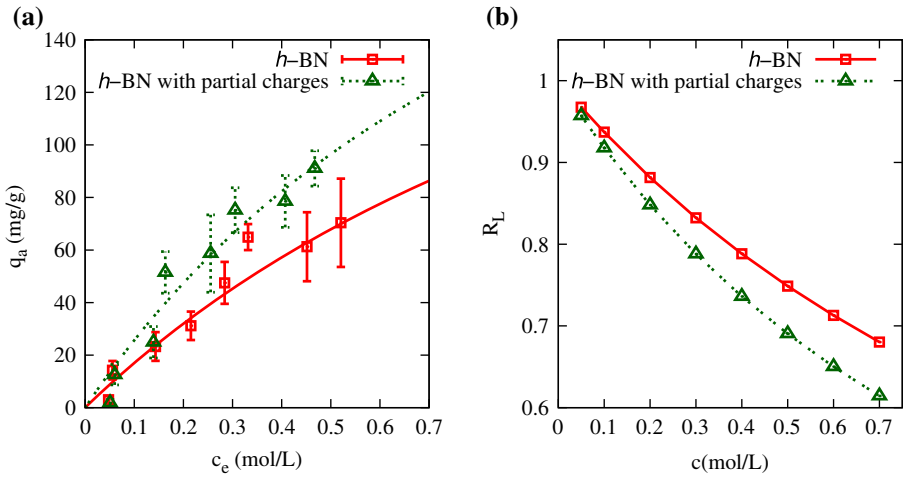

Figure 13. (Colour online) The Langmuir adsorption isotherm of arsenic ions (As^{3+}) (panel a) and equilibrium parameter (R_L) as a function of ion concentration (c) (panel b) on h-BN nanosheet with and without partial charges.

increasing q_a with increase in the ion concentration(Figure 5). The higher values of diffusion coefficient indicate weak adsorption behaviour of As^{3+} ions on graphene nanosheet, which is also apparent from the equilibrium parameter ($R_L > 0.9$).

Using molecular dynamic simulation, we can obtain information related to the impact of the nanosheet interaction on adsorption of ion by accessing dynamical behaviour of the system. The residence time is one such dynamical property that reveals time of stay of the ions near the nanosheet. This provides mechanistic information about the strength of interaction between the ions and the nanosheet. Therefore, we analyse the residence time of water and arsenic ion in the monolayer near the h-BN and graphene nanosheets by fitting the time correlation function Equation (4). The residence time of water increases from 150 ps to 240 ps with increasing ion concentration (see Figure 11(a)) and is almost similar in both the nanosheets. The residence time of As^{3+} ion also increases with increasing ion concentration in aqueous solution. In case of h-BN nanosheet, the residence time of arsenic ion is around 300 ps to 1000 ps (Figure 11(b)). Whereas in graphene nanosheet, the residence time of arsenic ions is found to be 10 ps to 350 ps which is one order less compared to that on h-BN nanosheet. The larger residence time obtained for the As^{3+} ions on h-BN nanosheet indicates that there is stronger interaction between arsenic ions and h-BN nanosheet. The larger residence time also corroborate the finding of the higher adsorption capacity of arsenic ion on h-BN nanosheet compared to graphene nanosheet.

To further understand the adsorption mechanism of arsenic ions on the nanosheets, we have calculated the PMF. PMF has been proved to be a useful quantity to explain the adsorption mechanism of the ions on the nanosheet. The PMF of arsenic ion adsorption is shown in Figure 12 as a function of distance from the nanosheets. It is observed that the PMF curve shows two distinct minima located around 4.5 and 7.5 Å, respectively. The first minima near the nanosheet are called the contact minima of ion and nanosheet and the second minima are called the solvent layer separated minima (SLSM). The PMF value at contact minima for arsenic ion in the presence of h-BN and graphene nanosheets are −1.35, and −1.2 kcal/mol, respectively, at 4.5 Å. The lower PMF value at contact minima indicates favourable adsorption of arsenic ion h-BN nanosheet compared to graphene nanosheet. At SLSM, the PMF values are −0.4 and −0.2 kcal/mol for h-BN and graphene nanosheets, respectively. It is observed from Figure 12 that there are two noticeable free energy barrier of adsorption at about 6 and 9 Åfrom the nanosheets. In case of h-BN nanosheet, an arsenic ion need to cross two free energy barriers of 0.2 and 1.2 kcal/mol to move from bulk to the nanosheet. Similarly in graphene nanosheet we observed two free-energy barriers, 0.15 and 0.8 kcal/mol for arsenic ion transfers from the bulk to the graphene nanosheet. For desorption of arsenic ion from the nanosheet to bulk shows two free energy barriers for both h-BN and graphene nanosheets. The desorption free energy barriers for arsenic ion on the h-BN nanosheet are 2.3 and 0.7 kcal/mol. In the presence of graphene nanosheet, the arsenic ion desorption free energy barriers are 1.5 and 0.5 kcal/mol. The lower adsorption and desorption energy barriers for arsenic ion in presence of graphene nanosheet promote arsenic ions to easily adsorb and desorb from the graphene nanosheet compared to the h-BN nanosheet. It is also observed that due to high desorption energy barrier, arsenic ion once adsorbed on the h-BN nanosheet is not desorbed readily.

The present study indicates h-BN nanosheet is superior adsorbent for As^{3+} ions in comparison to graphene nanosheet. However above analysis is based on zero partial charges on B and N atoms in the h-BN nanosheet, whereas several authors [29,70] reported that the partial charges on B and N are non-negligible. In order to investigate the influence of partial charges on h-BN nanosheet for adsorption of As^{3+} ions, we consider +0.35 and −0.35 charge on B and N, respectively [70]. In Figure 13(a), we have plotted the Langmuir adsorption isotherm of As^{3+} ions using h-BN nanosheets with and without partial charges on B and N atoms. It is clearly observed that the adsorption of As^{3+} ions are more on h-BN nanosheet with partial charges compared to zero charges on nanosheet. This is also evident from the equilibrium parameter (R_L) plot (see Figure 13(b)) showing comparatively favourable adsorption on h-BN nanosheets having partial charges. The maximum arsenic ion adsorption capacity (q_m) on h-BN nanosheet with partial charges is 311.7 mg/g.

4. Conclusions

Adsorption of arsenic ions on hexagonal boron nitride and graphene nanosheets has been studied using MD simulations. Adsorption of arsenic ions is found to be increased with increasing ion concentration and follows the Langmuir isotherm. The maximum adsorption capacity of arsenic ion is found to be 270.1 mg/g and 211.7 mg/g for *h*-BN and graphene nanosheets, respectively. Monolayer diffusion coefficients of water and ions near the *h*-BN and graphene nanosheets decrease with increasing ion concentrations. This indicates that the arsenic ion adsorption is more favourable on *h*-BN nanosheet which is also evident from the values of equilibrium parameter (R_L) obtained from the Langmuir isotherm. The potential of mean force (PMF) calculations revealed that arsenic ions need to overcome two energy barrier to adsorb on the nanosheet. The *h*-BN nanosheet possesses lower contact minima (−1.35 kcal/mol) for arsenic ion compared to graphene nanosheet (−1.2 kcal/mol), indicating that arsenic ions interact more strongly with *h*-BN nanosheet. The PMF of desorption of arsenic ions on *h*-BN nanosheet showed higher energy barrier (2.3 kcal/mol) than that on graphene nanosheet (1.5 kcal/mol). This implies that arsenic ion once adsorbed on *h*-BN nanosheet is difficult to exchange with the bulk solution. However, in case of graphene nanosheet the adsorbed arsenic ions can easily desorb due to the low energy barrier. The residence time of arsenic ion is threefold higher on *h*-BN nanosheet compared to the graphene nanosheet, which is well supported by the higher desorption barrier on *h*-BN nanosheet. The present study also suggests that the partial charges on B and N atoms in the *h*-BN nanosheet influence the adsorption isotherm of As^{3+} ions. There is 13% increment in the maximum As^{3+} ion adsorption capacity of *h*-BN having partial charges (311.7 mg/g) compared to uncharged *h*-BN. Our study clearly summarises that the *h*-BN nanosheet is a potential material for removing As^{3+} from aqueous media.

Funding

This work is supported by the Department of Science and Technology, Government of India [project number DST/TM/WTI/2K15/112]. The computational resources are provided by the HPC, Computer Center (CC), Indian Institute of Technology Kanpur. Author (RS) is thankful to A.K. Metya for fruitful discussion.

References

[1] World Health Organization. Guidelines for drinking water quality. Geneva, Switzerland: WHO Press; 2011.
[2] Rodríguez-Lado L, Sun G, Berg M, et al. Groundwater arsenic contamination throughout china. Science. 2013;341:866–868. Available from: http://science.sciencemag.org/content/341/6148/866
[3] Amini M, Abbaspour KC, Berg M, et al. Statistical modeling of global geogenic arsenic contamination in groundwater. Environ Sci Technol. 2008;42:3669–3675. doi:10.1021/es702859e.
[4] Fendorf S, Michael HA, van Geen A. Spatial and temporal variations of groundwater arsenic in south and southeast asia. Science. 2010;328:1123–1127. Available from: http://science.sciencemag.org/content/328/5982/1123
[5] Ravenscroft P, Brammer H, Richards K. Arsenic pollution: a global synthesis. Wiley; 2009. (RGS-IBG book series). Available from: https://books.google.co.in/books?id=1oPhSpFm6BMC
[6] Some drinking-water disinfectants and contaminants. including arsenic. 2004. (Vol. 84. IARC Monographs on the evaluation of carcinogenic risks to humans). Available from: http://monographs.iarc.fr/ENG/Monographs/vol84/
[7] Li W, Chen D, Xia F, et al. Extremely high arsenic removal capacity for mesoporous aluminium magnesium oxide composites. Environ Sci: Nano. 2016;3:94–106. doi:10.1039/C5EN00171D.
[8] Solé-Sardans M, Gamisans X, Dorado AD, et al. Exploring arsenic adsorption at low concentration onto modified leonardite. Water Air Soil Pollut. 2016;227:1–9. doi:10.1007/s11270-016-2827-x.
[9] Dai M, Xia L, Song S, et al. Adsorption of as(v) inside the pores of porous hematite in water. J Hazard Mater. 2016;307:312–317. Available from: http://www.sciencedirect.com/science/article/pii/S0304389416300085
[10] Katsoyiannis I, Zouboulis A, Althoff H, et al. As(iii) removal from groundwaters using fixed-bed upflow bioreactors. Chemosphere. 2002;47:325–332. Available from: http://www.sciencedirect.com/science/article/pii/S004565350100306X
[11] Mohan D, Pittman JCU. Arsenic removal from water/wastewater using adsorbentsa critical review. J Hazard Mater. 2007;142:1–53. Available from: http://www.sciencedirect.com/science/article/pii/S0304389407000349
[12] Jin Z, Jia Y, Zhang KS, et al. Effective removal of fluoride by porous mgo nanoplates and its adsorption mechanism. J Alloy Compd. 2016;675:292–300. Available from: http://www.sciencedirect.com/science/article/pii/S0925838816306879
[13] Yang X, Wang X, Feng Y, et al. Removal of multifold heavy metal contaminations in drinking water by porous magnetic fe2o3@alo(oh) superstructure. J Mater Chem A. 2013;1:473–477. doi:10.1039/C2TA00594H.
[14] Lata S, Samadder S. Removal of arsenic from water using nano adsorbents and challenges: a review. J Environ Manage. 2016;166:387–406. Available from: http://www.sciencedirect.com/science/article/pii/S0301479715303376
[15] Habuda-Stanić M, Nujić M. Arsenic removal by nanoparticles: a review. Environ Sci Pollut Res. 2015;22:8094–8123. doi:10.1007/s11356-015-4307-z.
[16] Setyono D, Valiyaveettil S. Chemically modified sawdust as renewable adsorbent for arsenic removal from water. ACS Sustainable Chem Eng. 2014;2:2722–2729. doi:10.1021/sc500458x.
[17] Nigam S, Gopal K, Vankar PS. Biosorption of arsenic in drinking water by submerged plant: hydrilla verticilata. Environ Sci Pollut Res. 2013;20:4000–4008. doi:10.1007/s11356-012-1342-x.
[18] Gupta A, Chauhan VS, Sankararamakrishnan N. Preparation and evaluation of iron-chitosan composites for removal of as(iii) and as(v) from arsenic contaminated real life groundwater. Water Res. 2009;43:3862–3870. Available from: http://www.sciencedirect.com/science/article/pii/S0043135409003558
[19] Chen W, Parette R, Zou J, et al. Arsenic removal by iron-modified activated carbon. Water Res. 2007;41:1851–1858. Available from: http://www.sciencedirect.com/science/article/pii/S0043135407000565
[20] Ogata F, Kawasaki N. Adsorption of as(iii) from aqueous solutions by novel fe-mg type hydrotalcite. Chem Pharm Bull. 2015;63:1040–1046.
[21] Lan J. Removal of arsenic from aqueous systems by use of magnetic fe3o4@tio2 nanoparticles. Res Chem Intermed. 2015;41:3531–3541. doi:10.1007/s11164-013-1469-5.
[22] Mandal S, Sahu MK, Patel RK. Adsorption studies of arsenic(iii) removal from water by zirconium polyacrylamide hybrid material (zrpacm-43). Water Resour Ind. 2013;4:51–67. Available from: http://www.sciencedirect.com/science/article/pii/S2212371713000401
[23] Zhang YX, Yu XY, Jin Z, et al. Ultra high adsorption capacity of fried egg jellyfish-like [gamma]-alooh(boehmite)@sio2/fe3o4 porous magnetic microspheres for aqueous pb(ii) removal. J Mater Chem. 2011;21:16550–16557. doi:10.1039/C1JM12196K.
[24] Li Q, Yang T, Yang Q, et al. Porous hexagonal boron nitride whiskers fabricated at low temperature for effective removal of organic pollutants from water. Ceram Int. 2016;42:8754–8762. Available from: http://www.sciencedirect.com/science/article/pii/S0272884216300566

[25] Gu J, Yuan S, Shu W, et al. PVBC microspheres tethered with poly(3-sulfopropyl methacrylate) brushes for effective removal of pb(ii) ions from aqueous solution. Colloid Surface A. 2016;498:218–230. Available from: http://www.sciencedirect.com/science/article/pii/S0927775716302114
[26] Li YH, Wang S, Luan Z, et al. Adsorption of cadmium(ii) from aqueous solution by surface oxidized carbon nanotubes. Carbon. 2003;41:1057–1062. Available from: http://www.sciencedirect.com/science/article/pii/S0008622302004402
[27] Li YH, Ding J, Luan Z, et al. Competitive adsorption of pb2+, cu2+ and cd2+ ions from aqueous solutions by multiwalled carbon nanotubes. Carbon. 2003;41:2787–2792. Available from: http://www.sciencedirect.com/science/article/pii/S0008622303003920
[28] Fornasiero F, Park HG, Holt JK, et al. Ion exclusion by sub-2-nm carbon nanotube pores. Proc Nat Acad Sci. 2008;105:17250–17255. Available from: http://www.pnas.org/content/105/45/17250.abstract
[29] Garnier L, Szymczyk A, Malfreyt P, et al. Physics behind water transport through nanoporous boron nitride and graphene. J Phys Chem Lett. 2016;7:3371–3376. pMID: 27504857. doi:10.1021/acs.jpclett.6b01365.
[30] Zhao J, Ren W, Cheng HM. Graphene sponge for efficient and repeatable adsorption and desorption of water contaminations. J Mater Chem. 2012;22:20197–20202. doi:10.1039/C2JM34128J.
[31] Wu T, Cai X, Tan S, et al. Adsorption characteristics of acrylonitrile, p-toluenesulfonic acid, 1-naphthalenesulfonic acid and methyl blue on graphene in aqueous solutions. Chem Eng J. 2011;173:144–149. Available from: http://www.sciencedirect.com/science/article/pii/S1385894711008771
[32] Mishra AK, Ramaprabhu S. Functionalized graphene sheets for arsenic removal and desalination of sea water. Desalination. 2011;282:39–45. current Development of Wastewater Treatment in India; Available from: http://www.sciencedirect.com/science/article/pii/S001191641100049X
[33] Hu X, Liu J, He Q, et al. Aqueous compatible boron nitride nanosheets for high-performance hydrogels. Nanoscale. 2016;8:4260–4266. doi:10.1039/C5NR07578E.
[34] Pakdel A, Bando Y, Golberg D. Nano boron nitride flatland. Chem Soc Rev. 2014;43:934–959. doi:10.1039/C3CS60260E.
[35] Guo H, Zhang W, Lu N, et al. Co2 capture on h-bn sheet with high selectivity controlled by external electric field. J Phys Chem C. 2015;119:6912–6917. doi:10.1021/acs.jpcc.5b00681.
[36] Sajjad M, Morell G, Feng P. Advance in novel boron nitride nanosheets to nanoelectronic device applications. ACS Appl Mater Interfaces. 2013;5:5051–5056. doi:10.1021/am400871s.
[37] Kubota Y, Watanabe K, Tsuda O, et al. Deep ultraviolet light-emitting hexagonal boron nitride synthesized at atmospheric pressure. Science. 2007;317:932–934. Available from: http://science.sciencemag.org/content/317/5840/932
[38] Sun W, Meng Y, Fu Q, et al. High-yield production of boron nitride nanosheets and its uses as a catalyst support for hydrogenation of nitroaromatics. ACS Appl Mater Interfaces. 2016;8:9881–9888. doi:10.1021/acsami.6b01008.
[39] Postole G, Gervasini A, Guimon C, et al. Influence of the preparation method on the surface characteristics and activity of boron-nitride-supported noble metal catalysts. J Phys Chem B. 2006;110:12572–12580. doi:10.1021/jp060183x.
[40] Weiwei L, Si Q, Dan L, et al. Large scale boron carbon nitride nanosheets with enhanced lithium storage capabilities. Chem Commun. 2013;49:352–354. doi:10.1039/C2CC36998B.
[41] Li J, Jin P, Tang C. Cr(iii) adsorption by fluorinated activated boron nitride: a combined experimental and theoretical investigation. RSC Adv. 2014;4:14815–14821. doi:10.1039/C4RA01684J.
[42] Li J, Jia H, Lin J, et al. Free-standing membranes made of activated boron nitride for efficient water cleaning. RSC Adv. 2015;5:71537–71543. doi:10.1039/C5RA11899A.
[43] Li J, Xiao X, Xu X, et al. Activated boron nitride as an effective adsorbent for metal ions and organic pollutants. Sci Rep. 2013;3:3208. doi:10.1038/srep03208.
[44] Zhang X, Lian G, Zhang S, et al. Boron nitride nanocarpets: controllable synthesis and their adsorption performance to organic pollutants. CrystEngComm. 2012;14:4670–4676. doi:10.1039/C2CE06748J.
[45] Lei W, Portehault D, Liu D, et al. Porous boron nitride nanosheets for effective water cleaning. Nat Commun. 2013;4:1777. doi:10.1038/ncomms2818.
[46] Chen R, Zhi C, Yang H, et al. Arsenic (v) adsorption on fe3o4 nanoparticle-coated boron nitride nanotubes. J Colloid Interface Sci. 2011;359:261–268. Available from: http://www.sciencedirect.com/science/article/pii/S0021979711002840
[47] Kumar S, Nair RR, Pillai PB, et al. Graphene oxide-mnfe2o4 magnetic nanohybrids for efficient removal of lead and arsenic from water. ACS Appl Mater Interfaces. 2014;6:17426–17436.
[48] Henke K, editor. Arsenic: environmental chemistry, health threats and waste treatment. 1st ed. Wiley; 2009.
[49] Zhang L, Zhu T, Liu X, et al. Simultaneous oxidation and adsorption of as(iii) from water by cerium modified chitosan ultrafine nanobiosorbent. J Hazard Mater. 2016;308:1–10. Available from: http://www.sciencedirect.com/science/article/pii/S0304389416300152
[50] Humphrey W, Dalke A, Schulten K. VMD - Visual Molecular Dynamics. J Mol Graph. 1996;14:33–38.
[51] Kang JW, Hwang HJ. Comparison of c_{60} encapsulations into carbon and boron nitride nanotubes. J Phys: Condens Matter. 2004;16:3901. Available from: http://stacks.iop.org/0953-8984/16/i=23/a=010
[52] Konatham D, Yu J, Ho TA, et al. Simulation insights for graphene-based water desalination membranes. Langmuir. 2013;29:11884–11897. doi:10.1021/la4018695.
[53] Mark P, Nilsson L. Structure and dynamics of the tip3p, spc, and spc/e water models at 298 k. J Phys Chem A. 2001;105:9954–9960. doi:10.1021/jp003020w.
[54] Rappe AK, Casewit CJ, Colwell KS, et al. Uff, a full periodic table force field for molecular mechanics and molecular dynamics simulations. J Am Chem Soc. 1992;114:10024–10035. doi:10.1021/ja00051a040.
[55] Minofar B, Vácha R, Wahab A, et al. Propensity for the air/water interface and ion pairing in magnesium acetate vs magnesium nitrate solutions: molecular dynamics simulations and surface tension measurements. J Phys Chem B. 2006;110:15939–15944. doi:10.1021/jp060627p.
[56] Anitha K, Namsani S, Singh JK. Removal of heavy metal ions using a functionalized single-walled carbon nanotube: A molecular dynamics study. J Phys Chem A. 2015;119:8349–8358. doi:10.1021/acs.jpca.5b03352.
[57] Jorgensen WL, Maxwell DS, Tirado-Rives J. Development and testing of the opls all-atom force field on conformational energetics and properties of organic liquids. J Am Chem Soc. 1996;118:11225–11236. doi:10.1021/ja9621760.
[58] Plimpton S. Fast parallel algorithms for short-range molecular dynamics. J Comput Phys. 1995;117:1–19. Available from: http://www.sciencedirect.com/science/article/pii/S002199918571039X
[59] Marry V, Rotenberg B, Turq P. Structure and dynamics of water at a clay surface from molecular dynamics simulation. Phys Chem Chem Phys. 2008;10:4802–4813. doi:10.1039/B807288D.
[60] Liu P, Harder E, Berne BJ. On the calculation of diffusion coefficients in confined fluids and interfaces with an application to the liquidvapor interface of water. J Phys Chem B. 2004;108:6595–6602. doi:10.1021/jp0375057.
[61] Chitra R, Yashonath S. Estimation of error in the diffusion coefficient from molecular dynamics simulations. J Phys Chem B. 1997;101:5437–5445. doi:10.1021/jp9703059.
[62] Bhandary D, Khan S, Singh JK. Structure and dynamics of n-alkanol monolayers on a mica surface. J Phy Chem C. 2014;118:6809–6819. doi:10.1021/jp412137w.
[63] Hall KR, Eagleton LC, Acrivos A, et al. Pore- and solid-diffusion kinetics in fixed-bed adsorption under constant-pattern conditions. Ind Eng Chem Fund. 1966;5:212–223. doi:10.1021/i160018a011.
[64] Taffarel SR, Rubio J. Removal of mn2+ from aqueous solution by manganese oxide coated zeolite. Miner Eng. 2010;23:1131–1138. Available from: http://www.sciencedirect.com/science/article/pii/S0892687510001767

[65] Roux B. The calculation of the potential of mean force using computer simulations. Comp Phys Comm. 1995;91:275–282. Available from: http://www.sciencedirect.com/science/article/pii/001046559500053I

[66] Souaille M, Roux B. Extension to the weighted histogram analysis method: combining umbrella sampling with free energy calculations. Comput Phys Commun. 2001;135:40–57. Available from: http://www.sciencedirect.com/science/article/pii/S0010465500002150

[67] Binder K, Baumgärtner A, Burkitt A, et al. The monte carlo method in condensed matter physics. Berlin Heidelberg: Topics in applied physics; Springer; 2012. Available from: https://books.google.co.in/books?id=-QX9CAAAQBAJ

[68] Dutta RC, Khan S, Singh JK. Wetting transition of water on graphite and boron-nitride surfaces: A molecular dynamics study. Fluid Phase Equilib. 2011;302:310–315. 12th International Conference on Properties and Phase Equilibria for Product and Process Design; Available from: http://www.sciencedirect.com/science/article/pii/S0378381210003663

[69] Werder T, Walther JH, Jaffe RL, et al. On the water-carbon interaction for use in molecular dynamics simulations of graphite and carbon nanotubes. J Phys Chem B. 2003;107:1345–1352.

[70] Tocci G, Joly L, Michaelides A. Friction of water on graphene and hexagonal boron nitride from ab initio methods: very different slippage despite very similar interface structures. Nano Lett. 2014;14:6872–6877. pMID: 25394228. doi:10.1021/nl502837d.